Whole lifespan microscopic observation of budding yeast aging through a microfluidic dissection platform

Lee, S S ; Vizcarra, I A ; Huberts, D H E W ; Lee, L P ; Heinemann, M

Abstract: Important insights into aging have been generated with the genetically tractable and short-lived budding yeast. However, it is still impossible today to continuously track cells by high-resolution microscopic imaging (e.g., fluorescent imaging) throughout their entire lifespan. Instead, the field still needs to rely on a 50-y-old laborious and time-consuming method to assess the lifespan of yeast cells and to isolate differentially aged cells for microscopic snapshots via manual dissection of daughter cells from the larger mother cell. Here, we are unique in achieving continuous and highresolution microscopic imaging of the entire replicative lifespan of single yeast cells. Our microfluidic dissection platform features an optically prealigned single focal plane and an integrated array of soft elastomer-based micropads, used together to allow for trapping of mother cells, removal of daughter cells, monitoring gradual changes in aging, and unprecedented microscopic imaging of the whole aging process. Using the platform, we found remarkable age-associated changes in phenotypes (e.g., that cells can show strikingly differential cell and vacuole morphologies at the moment of their deaths), indicating substantial heterogeneity in cell aging and death. We envision the microfluidic dissection platform to become a major tool in aging research.

DOI: https://doi.org/10.1073/pnas.1113505109

Whole Lifespan Microscopic Observation of Budding Yeast Aging through a Microfluidic Dissection Platform

Sung Sik Lee[1,2,*,†], Ima Avalos Vizcarra[1,*,‡], Daphne H. E. W. Huberts[3],

Luke P. Lee[2,§], Matthias Heinemann[1,3,¶]

[1] ETH Zurich, Institute of Molecular Systems Biology, Wolfgang-Pauli-Strasse 16, 8093 Zurich, Switzerland

[2]ETH Zurich, Department of Biosystems Science and Engineering, Mattenstrasse 26, 4058 Basel, Switzerland

[3]University of Groningen, Groningen Biomolecular Sciences and Biotechnology Institute, Molecular Systems Biology, Nijenborgh 4, 9747 AG Groningen, The Netherlands

* Equally contributing first authors

[†]Present address: ETH Zurich, Institute of Biochemistry, Schafmattstrasse 18, 8093 Zurich, Switzerland

[‡]Present address: ETH Zurich, Department of Materials, Wolfgang-Pauli-Strasse 10, 8093 Zurich, Switzerland

[§]Present address: Department of Bioengineering, University of California, Berkeley, United States of America

[¶]Corresponding author: m.heinemann@rug.nl (phone +31 50 363 8146)

Abstract

Important insights into aging have been generated with the genetically tractable and short-lived budding yeast. However, it is still impossible today to continuously track cells by high-resolution microscopic imaging (e.g. fluorescent imaging) throughout their entire lifespan. Instead, the field still needs to rely on a 50-year-old laborious and time-consuming method to assess the lifespan of yeast cells and to isolate differentially aged cells for microscopic snapshots via manual dissection of daughter cells from the larger mother cell. Here, we achieve for the first time continuous and high-resolution microscopic imaging of the entire replicative lifespan of single yeast cells. Our microfluidic dissection platform features an optically pre-aligned single focal plane and an integrated array of soft elastomer-based micropads; together allowing for trapping of mother cells, removal of daughter cells, monitoring gradual changes in aging and unprecedented microscopic imaging of the whole aging process. Using the platform, we found remarkable age-associated changes in phenotypes, e.g. that cells can show strikingly differential cell and vacuole morphologies at the moment of their deaths, indicating substantial heterogeneity in cell aging and death. We envision the microfluidic dissection platform to become a major tool in aging research.

Introduction

Aging is a complex gradual impairment of normal biological function caused by accumulation of molecular damage, finally culminating in death. Investigation of the genetically tractable and short-lived budding yeast *Saccharomyces cerevisiae* has yielded important insights into general eukaryotic aging: specific genes mediate aging (*e.g.SIR2*) (1-3) and dietary limitations can increase life span (4). Its replicative aging is considered an important model for aging in mitotically active cells (5, 6) with the replicative lifespan being defined as the number of daughter cells produced by a mother cell before the mother cell ceases dividing (Fig. 1A). Because of asymmetrical inheritance of damage to the mother (7), senescence factors are thought to accumulate in mother cells (8). Comprehensive analyses of age-associated phenotypes are considered to be instrumental in identifying the senescence factors (9, 10).

Analyzing the phenotype of replicative aging yeast cells, however, harbors a major technical challenge: continuous budding of the cells causes the original mother cells to be rapidly outnumbered by the exponentially increasing number of daughter cells and thus makes long-term tracking of the aging cell impossible (Fig. S1). Technologies for studying age-associated phenotypes of replicative aging yeast cells are still very limited (e.g. Ref. (11)), and until today the prime tool in yeast aging research is yet a 50-year-old dissection method (12), in which daughter cells are removed by microscopic micromanipulation with a needle from the larger mother cell on thick opaque culture pads (10, 13) (Fig. 1B). In a laborious and time-consuming manner - one lifespan experiment requiring several days of manual work for removing daughter cells after each mitotic cycle - such dissection allows assessment of the cell lifespan (10), or the isolation of single cells to generate microscopic snapshots of differentially aged cells. This

capability has, for example, led to the finding that the morphology of cells changes with age (9, 10, 12). However, due to several constraints, the conventional dissection method does not allow for high-resolution microscopic imaging (*e.g*. fluorescent imaging), and not for continuous tracking of cells throughout their complete lifespan, which would afford dynamic and essential insights into the phenotype of aging cells.

Unprecedented insights into single cells during aging would be possible with a method that allows for continuous high-resolution microscopic imaging of whole life-spans of yeast cells from their youth through senescence to death. The development of microfluidic devices has raised expectations for their capability to cultivate yeast cells in controlled environments with simultaneous and continuous microscopic observation (14, 15). Unfortunately, none of the currently existing microfluidic devices can be applied for long-term replicative aging studies. Respective devices are limited either by the number of generations over which mother cells can be monitored (typically eight) because of the exponential increase in the number of daughter cells retained in the microfluidic observation chambers (16-18), or by non-ideal optical properties imposed by the chip design (19).

In this work, we set out to solve this problem and developed a microfluidic dissection platform with a pre-aligned single focal plane for long-term live cell imaging of the complete replicative (and also chronological) lifespan of budding yeast cells. Similar to the classical dissection method, our platform also draws on the fact that the mother is larger than the bud cell (Fig. 1C). Yeast mother cells are trapped under soft elastomer (PDMS: polydimethylsiloxane)-micropad. A continuous medium flow through the device washes away emerging buds and at the same time ensures a defined and constant environment during the whole aging experiment. This soft elastomer-based “microfluidic

dissection platform" allows monitoring of the aging process of single cells from "young" to "death" (i.e., up to about 40 generations). In addition to offering the capability of performing lifespan analyses in a less laborious manner, the excellent optical properties of the chip permit in vivo fluorescence measurements during the entire lifespan.

Result and Discussion

Yeast mother cells are trapped under micropads (30 µm × 15 µm, Fig. 1C and D) that are arranged in an array-based format (Fig. 1E). The engineered height between the micropad and the glass cover slide is similar to the diameter of yeast cells (*i.e.*, 4–5 µm), realizing a pre-aligned single focal plane for long-term live cell imaging (Fig. 1C) Hydrostatic pressure, applied during the loading of the chip with cells (Fig. S2), lifts up the approximately 200 elastic PDMS micropads and allows the cells to pass beneath them. After the release of this pressure, cells are trapped underneath the pads (Fig. 1D, loading) without any detrimental effects on the cells (cf. Fig. S3). After cell loading (described in detail in Fig.S2), a continuous medium flow through the device (i) washes away emerging buds, which - because of their smaller size - are not held under the micropad (Fig. 1D culturing, dissection) and (ii) ensures a defined and constant environment during the whole aging experiment. A stable and long-term operation of the chip (> 5 days) is ensured by the overall chip's channel layout.

With this technology, it is possible to monitor – in a fully automated manner without intervention of the experimenter- approximately 50 single cells from birth to death (*i.e.*, up to about 60 generations) in a single experiment (cf. Movie S1), despite the fact that occasionally bud cells push neighboring mother cells away from the micropad. This number of cells is comparable with the number of cells observed in conventional

lifespan analysis (13). Fig. S4 shows the dynamics of the cell retention capacity of the chip. We found that the division time of single cells obtained with our device agrees well with findings in another, independent study (20) (71 ± 0.8 min; n = 206 for 1^{st}–3^{rd} divisions of wild-type cells at 30ºC in Synthetic Defined Media with the full amino acid complement), indicating that our setup allows for the generation of physiologically correct data. At this point, it is important to note that with our setup starting the experiment with newborn cells is not guaranteed, although considering the typical bud index distribution of an exponentially growing liquid culture (*i.e.*, 80% of the cells have never budded before, 12% once, 6% twice, 3% three times (21), the majority of loaded cells are still new or recently born cells.

We first asked whether we could use the device to generate classical lifespan data in a simpler and automated way than with the conventional microdissection method. For this, we loaded wild-type cells and recorded the division events and time of individual cells until all cells had entered senescence (after approx. 48 h). Further, we used a *SIR2* and a *FOB1* deletion strain, which are known to show a decreased (2) and increased replicative lifespan, respectively (7, 11, 22). In Fig. 2A, the viability of these strains is shown as a function of the number of buds produced. Consistent with data from conventional dissection analysis (2, 7, 22), the lifespan of the *SIR2* deletion mutant is significantly shorter than that of the wild-type strain ($median_{WT}$: 21 divisions vs. $median_{sir2}$: 11 divisions) and the lifespan of the *FOB1* deletion mutant is longer ($median_{fob1}$: 32 divisions). An exact one-to-one comparison of the lifespans obtained with the classical dissection method with the ones generated with our microfluidic section platform (when using identical pre-culture and medium conditions) demonstrates that our experimental system generates the identical lifespan data (Fig. S5). Moreover, at the same time we overcome other limitations of the classical dissection method: (i) our

method effaces the limitations of the agar gel pad required for cell growth during classical dissection and the long-working distance objective lens that severely limits the optical resolution with which cells can be imaged (Fig. 1B); and (ii) it negates the issue of local nutrient depletion and by-product production during the experiment as we can now realize absolutely constant nutritional conditions (*e.g.*, calorie restriction or non-calorie restriction) throughout the whole experiment through a constant supply with fresh medium.

In addition to the acquisition of lifespan data, the dynamic progression of the division times of single cells can easily be assessed with our setup. Consistent with earlier reports, we noted that the division time and deviation increased dramatically as the cells approached the end of their lives (12) (100 ± 4.1, 122 ± 6.4, and 151.2 ± 9.5 for wild-type cells at 3, 2, and 1 buds before death, respectively) (Fig. 2B). With our platform, it is possible to measure division time very precisely, which has been difficult with the classical dissection method: manual dissection requires a few minutes per cell, and in single experiments, approximately 40 cells need to be observed and dissected continuously.

The unprecedented feature of our platform is the possibility for continuous high-resolution imaging of individual yeast cells from birth to death (Movie S1). We exploited this capability to generate novel data on gradual changes in cellular and vacuolar morphology during the complete lifespan of individual cells; the latter was visualized by a GFP-tagged version of *VPH1* (a subunit of the vacuolar-ATPase) (Fig. 2C and D). Consistent with earlier observations made at distinct time points (23), we observed that the surface of the cells becomes more wrinkled with age (12, 24) (Movie S1). Also, both the cell and vacuole sizes gradually become larger as cells age with an increase in both

sizes during the last three divisions (Fig. 2C and D), a finding that parallels the earlier observed increase in division time (Fig. 2B). Of interest, the ratio between vacuole size and cell size increases towards the end of the lifespan, potentially indicating higher autophagy activity (25). Exploiting the fact that in some cases, bud cells are not immediately removed from the pads, we found that the mother cell typically produced ellipsoidal daughter cells even before the mother's own shape became ellipsoidal (e.g. 25^{th} and 26^{th} buds in Fig. 2E, and Movie S1). Of note, these daughter cells died even earlier than the mother (Fig. 2E). Intriguingly, daughter cells of old mothers were sometimes found to be larger than the respective mother cell (Fig. S6 and Movie S2).

Because we could now trace cells during their complete replicative lifespan with continuously recording phenotypic traits, we wanted to explore whether there is heterogeneity in the aging process and death pattern, an insight that remains elusive in studies of yeast cell aging at the population level (11). First, we found two cell morphologies directly before a cell's death (Fig. 3A, bottom panels) - a spherical shape (34.1%) or an ellipsoidal outline (pseudohyphae, 65.9%) (Fig. 3A). Next, we focused on the vacuole morphology and identified three typical vacuole morphologies right before cell death: a tubular shape, a fused appearance, or a fragmented structure (Fig. 3B). Often, even a completely ruptured vacuole was observed at the end of a cell's life (Movies S1, S3, & S4). As intuitionally expected, the tubular structure was observed only with the ellipsoidal death pattern (Fig. 3B and C). This type of cell death points to problems in cytokinesis (26, 27), which may also cause failure of vacuole segregation. Usually, after a normal cell division, vacuole structures fuse and form one vacuole (cf. middle panel of Fig. 3B). However, in about 22% of all cases (Fig. 3C), this fusion fails or is not completed and fragmented vacuolar structures are observed at cell death (Fig. 3B, right panel).

With this heterogeneity in morphologies identified, we next asked whether the death types are correlated with any other measures that we obtained. Indeed, we found that cells dying with the spherical death type die – on average - at a younger age (after 12 buds generated) compared to cells dying the ellipsoidal death (after 23 buds generated) (Fig. 3D) and do so after a sudden increase in their cell sizes (Fig. 3E). This finding implies that the spherical cell death occurs rather at the mid age, suddenly "striking" young cells, while the ellipsoidal death occurs at rather an older age. This indicates that there is indeed heterogeneity in the aging process, resulting in fundamentally different culminations of damage that is ultimately incompatible with life. This fact underlines the importance of the developed platform for future yeast aging research.

Conclusion

In this paper, we present a microfluidic dissection platform that allows to track single yeast cells over their entire replicative (and chronological) lifespans with high-resolution imaging capability – a possibility the yeast aging research community has long awaited for. Not only can this technology replace the tedious manual microdissection methods to determine lifespan data, but it can also be used for high-resolution *in vivo* fluorescence imaging of aging cells under exactly controlled environmental conditions. It thus opens up unique possibilities for future aging research: Its capability for phenotypic tracing is essential (i) to explore the relevance of cell-to-cell heterogeneity in the aging process, and (ii) to address important questions such as whether certain phenotypes in cellular youth affect old-age behavior, or how damage is asymmetrically inherited by the mother cell and removed from the daughter cell and how this changes with age. We envision

that our technology will enable novel investigations in the quest for molecular mechanisms underlying the aging process and will permit large-scale screens into the aging phenotype for its capability to be easily multiplexed and to allow aging experiments in an unsupervised manner.

Methods

Yeast strain

All yeast strains used in this work were in the S288C (BY) background. The *SIR*2 and *FOB1* deletion strains were obtained from the yeast genome deletion collection, and the relevant genotype of the strain for visualization of the vacuole and MSN2 was *VMA*5-*RFP*::*KAN*^{R}; *VPH1-GFP*::*HIS3,*and *HOG1-mCherry:HIS3;* and *HTA2-CFP* with pRS315 MSN2-GFP plasmid, respectively. Yeast cells were prepared in Synthetic Defined Media with 2% glucose or Yeast Peptone Dextrose (YPD). Yeast cell cultures were grown overnight to stationary phase and then allowed to resume exponential growth by dilution into fresh growth medium (OD_{600} = 0.3), and incubation for 3 h at 30°C before the experiment. They were mildly sonicated for 1 min to separate any cell aggregates that could block the microfluidic device. The cells were then introduced into the microfluidic chamber.

Microfluidic device

The microfluidic device is made of PDMS (Sylgard 184, Dow Corning) and produced by replica molding from an SU-8 wafer. It consists of a main channel (height = 15 μm), which contains an array of micropads with a distance of 4 μm between the PDMs and glass slide, and a side channel (height = 100 μm) as a cell outlet during the loading process (Fig. S2). The microstructures were fabricated by photolithography using negative photoresists (SU-8 2002, and SU-8 10, Microchem Corp.). The side channel mold was made by adhesive tape. In a 1:10 w/w ratio, the PDMS base and curing agent were mixed, thoroughly stirred, and degassed in a vacuum chamber for 0.5–1 h to

remove air bubbles. The degassed mixture was poured onto the SU-8 master mold and cured on a hot plate (65°C for 1 h and 130°C for 30 min). The cured PDMS was carefully peeled off the mold. Inlet and outlet connections/holes were punched using a blunt injection needle. Finally, the surfaces of a cover glass and the PDMS mold were subjected to UV irradiation (UV Ozone cleaner PSD-UVT, Novascan) for 6 min to activate the surface for covalent bonding. The mask design required to produce the devices will be made available upon request.

Live cell imaging and analysis

The microfluidic device was mounted on the stage of an inverted microscope (Eclipse Ti, Nikon Instruments). Yeast cell growth and individual budding events were monitored by time-lapse imaging, successively capturing images every 10 min. The budding events are determined by comparison of two adjacent images, and the moment of cell death was identified by a sudden shrinkage of the cell's body. The hardware-based focusing system (Nikon Instruments: Perfect Focus System (PFS)) automatically and stably maintained the focus during the whole experiment. LED (pE2, CoolLed) illumination was used as the fluorescent light source. The images were taken with a high numerical aperture oil immersion objective lens (CFI Plan Apo 60X, Nikon; N.A. = 1.4; Working distance = 0.13 mm). The exposure times were 1 ms and 50 ms for transmission and GFP images, respectively. Defocused as well as focused transmission images were taken for subsequent segmentation of cells (28). The images were converted into binary images by manual application of the threshold function to ensure proper cell segmentation. The size of segmented cells was measured by the image process function in ImageJ (Wayne Rasband, National Institutes of Health, Bethesda, MD).

Acknowledgments

This work was supported by an Interdisciplinary Pilot Project (IPP) and the YeastX project within the Swiss Initiative in Systems Biology (SystemsX.ch) as well as by the Dutch Science Foundation (NWO)-funded Groningen Systems Biology Center for Energy Metabolism and Aging. The authors would like to thank Matthias Peter and Uwe Sauer for generously allowing use of the microscope, Dino Di Carlo and Ralf Streichan for helpful discussions, Andreas Hierlemann for generously allowing use of the cleanroom facility, Reinhard Dechant, Alessandro Baldi, Annina Denoth, and Serge Pelet for helpful discussions and donation of the yeast strain, and Ida van der Klei, Liesbeth Veenhof, and Yves Barral for excellent comments on the manuscript.

AUTHOR CONTRIBUTIONS

S. S. L. conceived the idea, developed the design, fabricated the microfluidic structure, and performed experiments; I. A. V. improved the designed and performed experiments; D. H. E. W. H. performed experiments; L. P. L. conceived the concept of live cell imaging in a single focal plane; M. H. conceived the idea and supervised the study. All authors wrote the manuscript.

References

1. Finkel T, Deng CX, & Mostoslavsky R (2009) Recent progress in the biology and physiology of sirtuins. Nature 460(7255):587-591.
2. Kaeberlein M, McVey M, & Guarente L (1999) The SIR2/3/4 complex and SIR2 alone promote longevity in Saccharomyces cerevisiae by two different mechanisms. Gene Dev 13(19):2570-2580.
3. Rine J (2005) Twists in the tale of the aging yeast. Science 310(5751):1124-1125.
4. Fontana L, Partridge L, & Longo VD (2010) Extending Healthy Life Span-From Yeast to Humans. Science 328(5976):321-326.
5. Gershon H & Gershon D (2000) The budding yeast, Saccharomyces cerevisiae, as a model for aging research: a critical review. Mech Ageing Dev 120(1-3):1-22.
6. Kaeberlein M (2010) Lessons on longevity from budding yeast. Nature 464(7288):513-519.
7. Shcheprova Z, Baldi S, Frei SB, Gonnet G, & Barral Y (2008) A mechanism for asymmetric segregation of age during yeast budding. Nature 454(7205):728-764.
8. Henderson KA & Gottschling DE (2008) A mother's sacrifice: what is she keeping for herself? Curr Opin Cell Biol 20(6):723-728.
9. Powell CD, Van Zandycke SM, Quain DE, & Smart KA (2000) Replicative ageing and senescence in Saccharomyces cerevisiae and the impact on brewing fermentations. Microbiology-Uk 146:1023-1034.
10. Steffen KK, Kennedy BK, & Kaeberlein M (2009) Measuring replicative life span in the budding yeast. J Vis Exp 28:1209.

11. Lindstrom DL & Gottschling DE (2009) The Mother Enrichment Program: A Genetic System for Facile Replicative Life Span Analysis in Saccharomyces cerevisiae. Genetics 183(2):413-422.
12. Mortimer RK & Johnston JR (1959) Life Span of Individual Yeast Cells. Nature 183(4677):1751-1752.
13. Medvedik O & Sinclair DA (2007) Caloric Restriction and Life Span Determination of Yeast Cells. Biological Aging: Methods and Protocols, (Springer), Vol 371, pp 97-109.
14. Lee PJ, Helman NC, Lim WA, & Hung PJ (2008) A microfluidic system for dynamic yeast cell imaging. Biotechniques 44(1):91-95.
15. Taylor RJ, et al. (2009) Dynamic analysis of MAPK signaling using a high-throughput microfluidic single-cell imaging platform. Proc Natl Acad Sci USA 106(10):3758-3763.
16. Cookson S, Ostroff N, Pang WL, Volfson D, & Hasty J (2005) Monitoring dynamics of single-cell gene expression over multiple cell cycles. Mol Syst Biol 1: 2005.0024.
17. Falconnet D, et al. (2011) High-throughput tracking of single yeast cells in a microfluidic imaging matrix. Lab Chip 11(3):466-473 .
18. Rowat AC, Bird JC, Agresti JJ, Rando OJ, & Weitz DA (2009) Tracking lineages of single cells in lines using a microfluidic device. Proc Natl Acad Sci USA 106(43):18149-18154.
19. Ryley J & Pereira-Smith OM (2006) Microfluidics device for single cell gene expression analysis in Saccharomyces cerevisiae. Yeast 23(14-15):1065-1073.

20. Charvin G, Cross FR, & Siggia ED (2008) A Microfluidic Device for Temporally Controlled Gene Expression and Long-Term Fluorescent Imaging in Unperturbed Dividing Yeast Cells. Plos One 3(1):e1468.

21. Vanoni M, Vai M, Popolo L, & Alberghina L (1983) Structural heterogeneity in populations of the budding yeast Saccharomyces cerevisiae. J Bacteriol 156(3):1282-1291.

22. Defossez PA, et al. (1999) Elimination of replication block protein Fob1 extends the life span of yeast mother cells. Mol Cell 3(4):447-455.

23. Egilmez NK, Chen JB, & Jazwinski SM (1990) Preparation and Partial Characterization of Old Yeast-Cells. Journals of Gerontology 45(1):B9-B17.

24. Muller I (1971) Experiments on Ageing in Single Cells of Saccharomyces-Cerevisiae. Archiv Fur Mikrobiologie 77(1):20-25.

25. Madeo F, Tavernarakis N, & Kroemer G (2010) Can autophagy promote longevity? Nat Cell Biol 12(9):842-846.

26. Barral Y, Parra M, Bidlingmaier S, & Snyder M (1999) Nim1-related kinases coordinate cell cycle progression with the organization of the peripheral cytoskeleton in yeast. Genes Dev 13(2):176-187.

27. Shulewitz MJ, Inouye CJ, & Thorner J (1999) Hsl7 localizes to a septin ring and serves as an adapter in a regulatory pathway that relieves tyrosine phosphorylation of Cdc28 protein kinase in Saccharomyces cerevisiae. Molecular and Cellular Biology 19(10):7123-7137.

28. Gordon A, et al. (2007) Single-cell quantification of molecules and rates using open-source microscope-based cytometry. Nature Methods 4(2):175-181.

List of Figures

Figure 2 Whole lifespan monitoring of cells. (A) Replicative lifespan analysis with novel platform. Cell viabilities are plotted as a function of number of buds produced (replicate lifespan). The lifespan of the *SIR2* gene deletion mutant (*sir2Δ*, n = 63) is shorter than that of the wild-type (WT, n = 76) and, that of the *FOB1* gene deletion mutant (*fob1Δ*, n = 58) is longer. **(B) Division time of WT, *sir2Δ, and fob1Δ.*** The plot shows the progression of the division time of WT, *sir2Δ*, and *fob1Δ* when the traces of the individual cells are normalized to the last division. ("†"represents death, error bar: mean ± SEM. **(C) Quantification of vacuole and cell size increase.** Near the end of the replicative lifespan the sizes and the ratio of vacuole and cell increase. **(D) Visual impression of increase in vacuole and cell size.** The upper panel showing bright-field images of a tracked cell at the 1st, 6th, 16th, and 26th generation. The lower panel shows the corresponding vacuole structures with fluorescent imaging using cells expressing Vph1p-GFP. **(E) Daughter cells from old mothers can die earlier than the mothers.** Black, gray and white arrows indicate the 25th, 26th, and 27th buds from the mother, respectively. The provided times indicate the durations of the cultivation.

Figure 3 Age-associated phenotypes. (A) Example images of cell morphology at the last division (upper part) and death (lower part). Cells either show a spherical shape (spherical) or form pseudohyphae (ellipsoidal). **(B) Example images of vacuole morphology before death.** Cells expressing Vph1p-GFP served for visualizing the vacuolar structure. Vacuoles form either a tubular-like, fused, or fragmented structure. The scale bar denotes 5μm. **(C) Distribution of age-associated phenotypes categorized by cell and vacuole morphologies at the last moment before death.** Outer ring, vacuole morphology; inner ring, cell morphology. **(D) Age-distribution at the**

two types of deaths. Upper panel, spherical death pattern (n =49, median = 12); lower panel, ellipsoidal death pattern (n=74, median =23). **(E) Dynamic change of the cell size in the two populations.** Left panel, cells that show spherical death pattern; right, cells that show ellipsoidal death pattern.

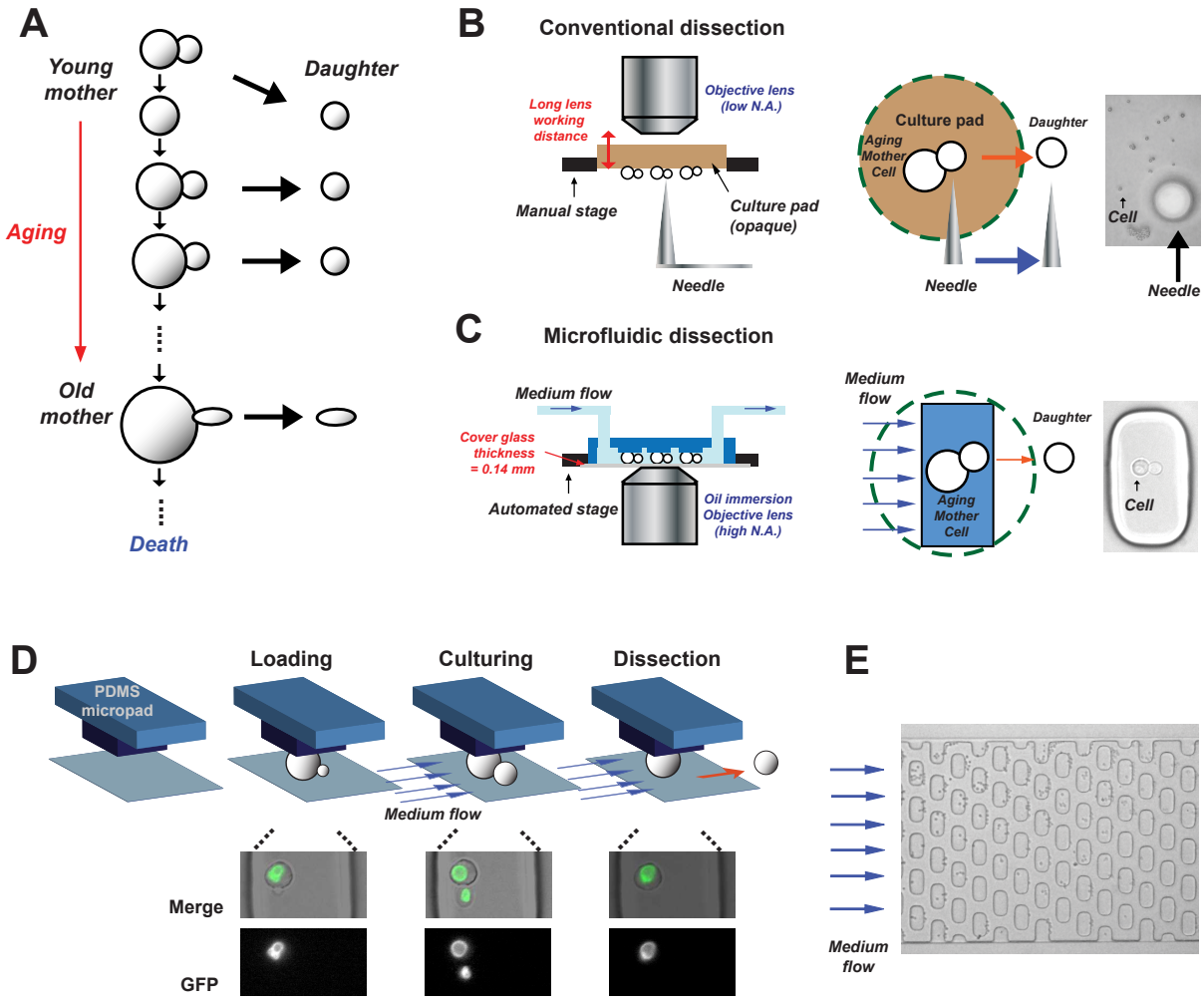
A
Young mother
Daughter
Aging
Old mother
Death
B
Conventional dissection
Long lens working distance
Objective lens (low N.A.)
Manual stage
Culture pad (opaque)
Needle
Culture pad
Daughter
Aging Mother Cell
Needle
Cell
Needle
C
Microfluidic dissection
Medium flow
Cover glass thickness = 0.14 mm
Automated stage
Oil immersion Objective lens (high N.A.)
Medium flow
Daughter
Aging Mother Cell
Cell
D
Loading
Culturing
Dissection
PDMS micropad
Medium flow
Merge
GFP
E
Medium flow

Figure 1

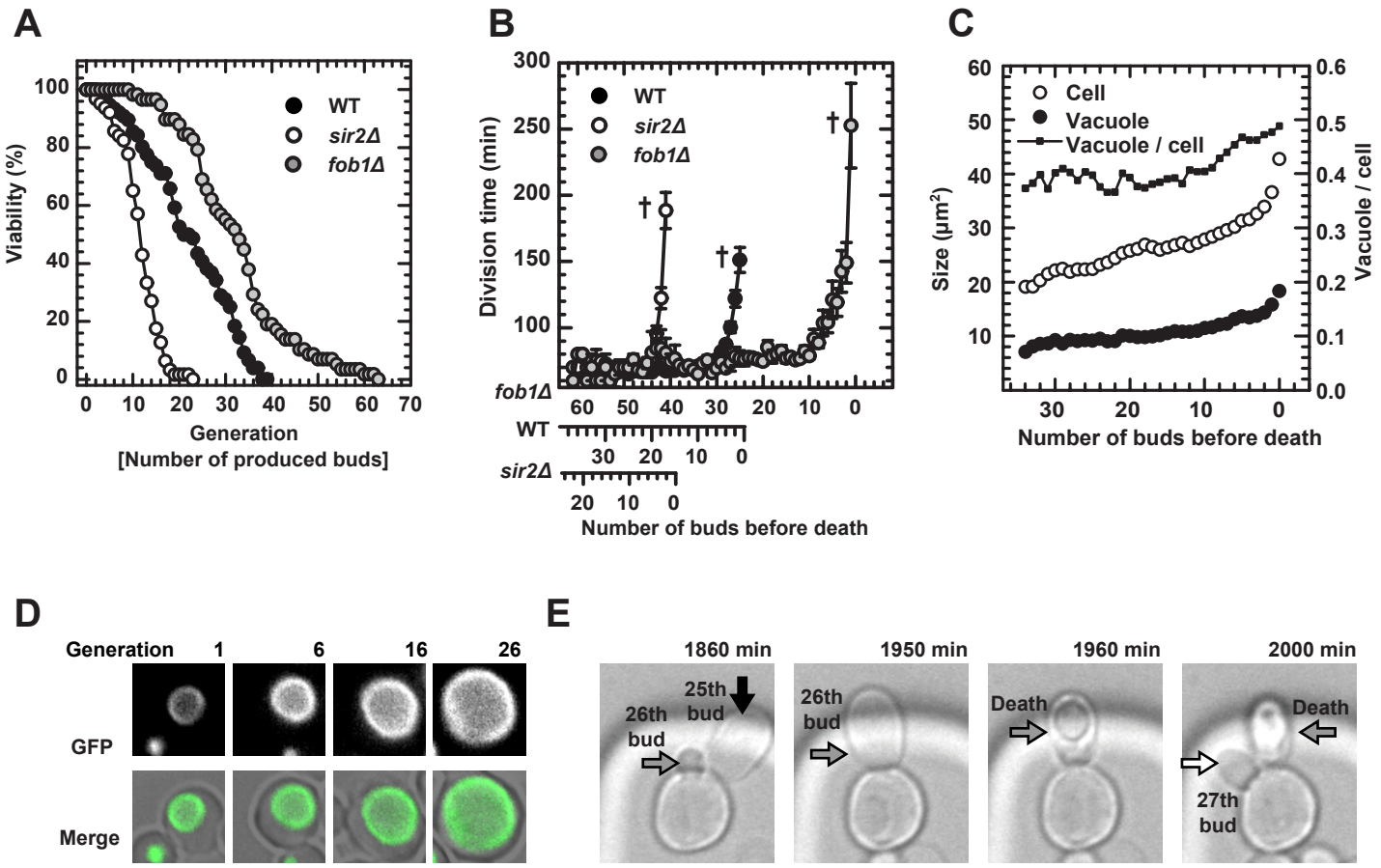
A
Viability (%)
Generation
[Number of produced buds]
WT
sir2Δ
fob1Δ
B
Division time (min)
fob1Δ
WT
sir2Δ
Number of buds before death
C
Cell
Vacuole
Vacuole / cell
Size (μm²)
Vacuole / cell
Number of buds before death
D
Generation 1 6 16 26
GFP
Merge
E
1860 min
1950 min
1960 min
2000 min
25th bud
26th bud
Death
27th bud

Figure 2

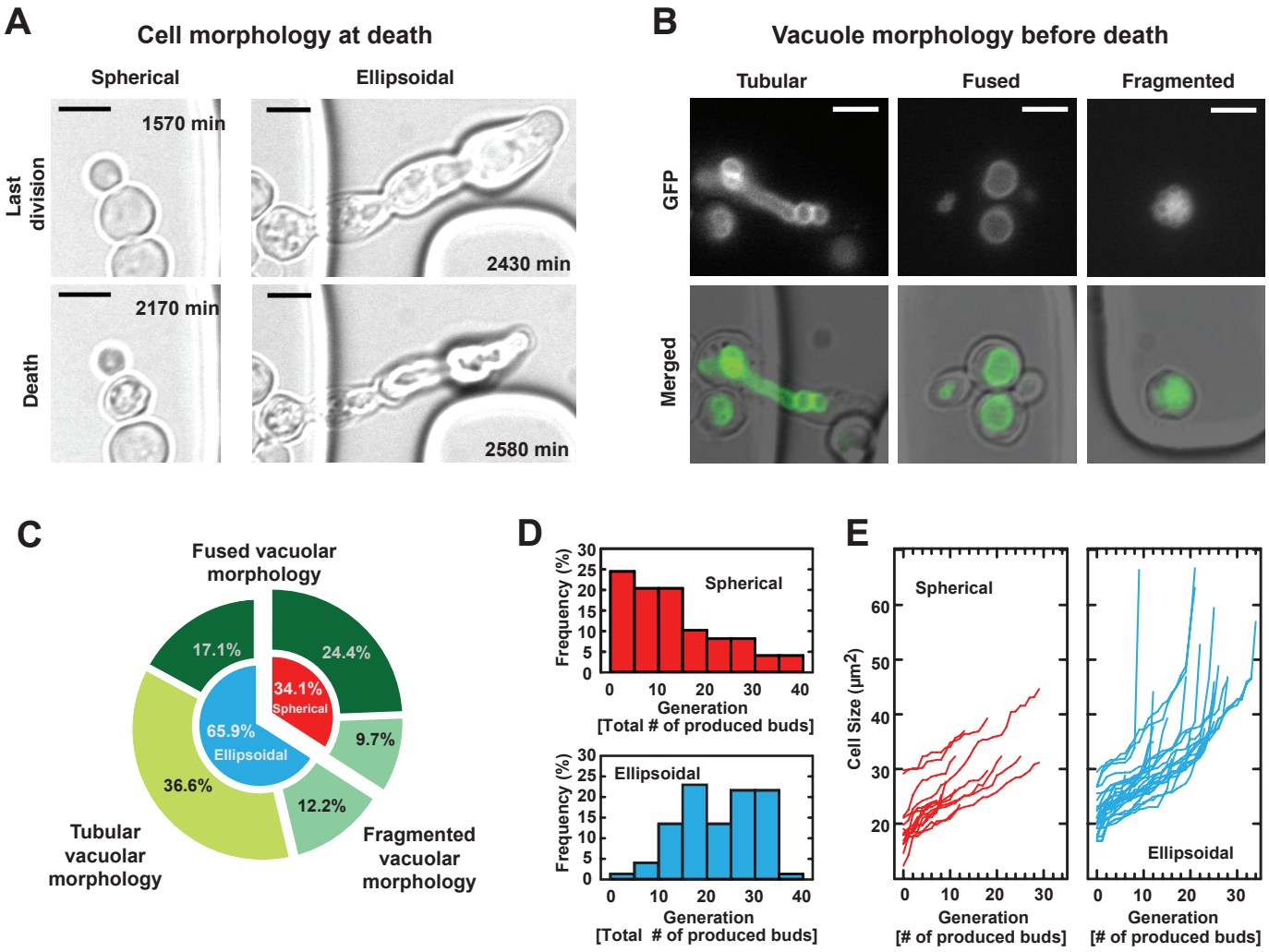
A
Cell morphology at death
Spherical
Ellipsoidal
Last division
Death
1570 min
2430 min
2170 min
2580 min
B
Vacuole morphology before death
Tubular
Fused
Fragmented
GFP
Merged
C
Fused vacuolar morphology
17.1%
24.4%
34.1%
Spherical
65.9%
Ellipsoidal
9.7%
36.6%
12.2%
Tubular vacuolar morphology
Fragmented vacuolar morphology
D
Frequency (%)
Spherical
Generation
[Total # of produced buds]
Ellipsoidal
E
Cell Size (μm2)
Spherical
Ellipsoidal
Generation
[# of produced buds]

Figure 3